JOURNAL OF GEOPHYSICAL RESEARCH, VOL. 113, F04002, doi:10.1029/2007JF000938, 2008

Evolution of sediment accommodation space in steady state bedrock-incising valleys subject to episodic aggradation

Stephen T. Lancaster[1]

Received 5 November 2007; revised 1 July 2008; accepted 22 August 2008; published 7 October 2008.

[1] Steepland valleys subject to debris flows incise bedrock even as episodic deposition typically covers valley bottoms. This paper's hypothesis is that, while continual fluvial processes evacuate deposits, storage of episodic deposition drives valley widening and, thereby, creation of accommodation space for sediment storage on the valley floor. Data from three headwater valleys in the Oregon Coast Range show that valley-to-channel width ratios and valley bottom deposit depths are variable, have little systematic variation with respect to contributing area, and are similar on average among sites. A model of valley cross-section evolution couples soil production, nonlinear diffusion, contrasting rates of channel incision into deposits and bedrock, and stochastic valley bottom deposition. The model reproduces observed flat, deposit-covered valley bottoms and abrupt transitions to valley sides with oversteepened toe slopes. Simulations address sensitivity of valley morphologies and incision rates to dimensionless numbers, the ratio of instantaneous bedrock and deposit erosion rates (incision number), and the ratio of deposition and evacuation rates (deposition number). For steady state simulations, increasing deposition number by $<10^1$ leads to deposit depth and valley bottom width increasing by 10^1 and $10^{1.5}$, respectively, and valley bottom incision relative to the instantaneous rate decreasing by 10^{-3}. For incision number increasing by 10^3, valley capacity (width times toe slope height) relative to mean deposit volume increases by $10^{1.5}$. Simulations, consistent with field data, imply that steady state valley widths are adjusted to episodic deposition rates and respond more quickly to changes than profile gradients because of contrasting limitations by instantaneous versus long-term lowering rates.

Citation: Lancaster, S. T. (2008), Evolution of sediment accommodation space in steady state bedrock-incising valleys subject to episodic aggradation, *J. Geophys. Res.*, *113*, F04002, doi:10.1029/2007JF000938.

1. Introduction

[2] In active orogens where landslides and debris flows are common, hillslopes and valleys are coupled in two ways, as identified by *Hovius et al.* [2000]: (1) valley lowering, especially by fluvial incision, drives steepening and promotes landslides and debris flows and (2) those landslides and debris flows supply, even inundate, the valleys with sediment that must be evacuated, typically by fluvial processes, in order for valley lowering to proceed [*Rice and Church*, 1996; *Lancaster and Grant*, 2006]. *Stock and Dietrich* [2003] found that up to 80% of mountain valley networks are dominated by debris flow scour and identified a transition to fluvial process dominance at gradients of 0.03–0.10. Because the frequency and magnitude characteristics of debris flow and fluvial processes are different, the transition from the former to the latter necessitates storage of debris flow and debris dam-impounded deposits until fluvial action removes them. For example, *Lancaster and Casebeer* [2007] found that 15% of basin sediment production was stored for, on average, 1.0 ka on a 2600 m length of valley bottom (Bear Creek; Table 1) in the Oregon Coast Range (OCR). And, as debris flow-dominated valleys can compose as much as 80% of the valley network in some landscapes, sediment storage at these valleys' transition to fluvial process dominance must represent a significant, if not the major, portion of nonhillslope sediment storage in many drainage basins and contribute greatly to the residence time of sediment in mountain drainage basins.

[3] In the Oregon Coast Range's Tyee Formation, the example addressed in this study, the combination of interbedded sandstones and mudstones [*Peck*, 1961] that weather into gravelly colluvium and the predominantly low-intensity rainfall produce a high density of small "hollows" (steep, unchanneled valleys) that produce sediment mainly by shallow rapid landslides that are generally channelized to form debris flows [e.g., *Montgomery et al.*, 2000]. Debris flow deposits are therefore prevalent throughout drainage networks in this formation and commonly create valley-spanning deposits with steep fronts composed of large wood (e.g., 1 m diameter) and boulders [e.g., *Lancaster et al.*, 2003; *Lancaster and Grant*, 2006] where valley widths are

[1]Department of Geosciences, Oregon State University, Corvallis, Oregon, USA.

0148-0227/08/2007JF000938$09.00

Table 1. Drainage Basin Characteristics for the Study Sites

Site	Surveyed Reach Length (m)	Drainage Area (km^2)	Elevation Range (m)	Contributing Area at Slope-Area Inflection Point[a] (m^2)	Stream Gradient at Slope-Area Inflection Point	Valley Bottom Sediment Depth[b] (m)	Ratio of Valley Bottom Width to Channel Width[c]
Cedar Creek	1240	1.86	79–539	1.12×10^6	1.21×10^{-1}	1.83 ± 0.97	6.28 ± 2.96
Hoffman Creek	2590	2.06	10–265	5.36×10^5	6.90×10^{-2}	2.10 ± 0.93	6.56 ± 2.75
Bear Creek	2660	2.23	97–480	1.07×10^6	1.05×10^{-1}	1.31 ± 0.75	5.02 ± 2.06

[a]Slope-area inflection point determined by Method 1 of *Stock and Dietrich* [2003].
[b]Average plus or minus standard deviation for nonzero depths, defined as cross-sectional area divided by valley bottom width measured on the deposit surface. Should be considered minimum estimates for Cedar and Hoffman.
[c]Average plus or minus standard deviation; values exclude locations with zero sediment storage.

less than or comparable to the lengths of the larger wood pieces (e.g., 40–80 m [*Garman et al.*, 1995]).

[4] In this study, I examine the coupling between episodic sediment supply by debris flows and continuous fluvial evacuation and, specifically, the implications of this coupling for the evolution of accommodation space through adjustment of valley width and inner gorge depth over geologic time. Although I focus on debris flows as depositional agents, the concepts addressed are more broadly applicable to any episodic deposition that temporarily overwhelms transport capacity, e.g., infilling behind debris dams [e.g., *Montgomery et al.*, 2003; *Lancaster and Grant*, 2006]. Also, although evacuation may sometimes be episodic, as in scour by debris flows, the breaching of debris dams, or even rapid fluvial incision during large storms, my treatment of continuous fluvial evacuation should effectively represent many situations in which there is some finite time between episodic deposition and subsequent uncovering and erosion of bedrock.

[5] Accommodation space as a control on deposition in sedimentary basins is well established [e.g., *Schlager*, 1993; *Muto and Steel*, 1997], and basin width is recognized among the controls on accommodation space and, therefore, alluvial fan size [*Weissmann et al.*, 2005]. Landslide sediment storage and evacuation have received some attention, but studies have focused on sediment fluxes at orogen margins and considered only short-term ($\sim 10^0$ a) storage of landslide-derived sediment in the mountain valley network [*Allen and Hovius*, 1998; *Hovius et al.*, 2000]. Recent work has begun to address the longer-term ($\sim 10^3$ a) storage of landslide-derived sediment in mountain valleys [*Lancaster and Casebeer*, 2007], but the potential influence of sediment supply on the evolution of accommodation space in active orogens has received little, if any, study.

[6] Previous study suggests that sediment deposited in headwater valleys of the OCR by episodic debris flows has mean transit times on the order of hundreds of years and that some sediments remain in storage on these valley floors for millennia [*Lancaster and Casebeer*, 2007]. While these sediment reservoirs comprise deposits throughout ~1 km valley reaches, the relevant spatial scales associated with the reservoirs and sediment transit times may often be the valley widths (10^1–10^2 m): some material eroded from valley bottoms by debris flows is subsequently deposited elsewhere in the same reach, but much, perhaps most, of the eroded sediment enters the channel and quickly (relative to the mean transit time) passes out of the reach [*Lancaster and Casebeer*, 2007]. Whereas some deposits have depths approaching 10 m, deposit depths on these valley floors are typically 1–2 m on average [*Miller and Benda*, 2000; *Lancaster and Casebeer*, 2007]. Moreover, deposit age estimates and sedimentary facies associations are consistent with steady state sediment storage volumes over times on the order of 10^2–10^3 a [*Lancaster and Casebeer*, 2007]. That is, over such periods average volumes may be nearly constant, even while volumes over shorter periods fluctuate because of episodic deposition and subsequent evacuation.

[7] *Lancaster and Grant* [2006] found that widths of headwater channels (Cedar, Hoffman, and Bear Creek sites; Table 1) in the OCR were, on average, only one-fifth the width of their valleys, even where those channel beds were bedrock. Wide valleys underlain by bedrock straths imply that the rate of lateral erosion is large relative to the rate of vertical incision due to sediment supply that is large relative to transport capacity such that the bed is often shielded [*Hancock and Anderson*, 2002; *Formento-Trigilio et al.*, 2003]. Models of strath formation have typically invoked continuous lateral erosion by meandering streams [e.g., *Hancock and Anderson*, 2002], but I reason that such continuous erosion is unnecessary and that, instead, straths may form by discrete changes in lateral channel position, as in the case of minor avulsions, as long as the frequency of those changes is large relative to the rate of vertical incision of bedrock.

[8] The central hypothesis of this paper is the following: if the landscape represents a steady state between uplift and incision, then existing valley morphologies, even where those valleys appear to be wide and aggraded, may also represent a steady state between incision and rock uplift while providing accommodation space for episodic, valley bottom-inundating deposition. In this paper, field data and observations will show that, in valleys in the OCR field sites at the transition between debris flow and fluvial processes, valley-to-channel width ratios and valley bottom sediment depths are highly variable along individual profiles, have no generalizable systematic variation downstream, but some consistency among sites on average. Analysis of unit stream power and sediment volumes will show that some channels may have adjusted to greater episodic supply.

[9] The major focus of the paper is on elucidating valley adjustments to episodic sediment supply with a simple cross-sectional model linking hillslope soil production and transport, stochastic valley bottom deposition and channel avulsion, and contrasting rates of channel incision into deposits and bedrock. Does episodic sediment supply drive the evolution of accommodation space for sediment on the valley bottom? Can valleys with different episodic sediment supplies and morphological adjustments, such as are observed at the field sites, still incise at the same rate? Can such valleys attain a steady state in which valley

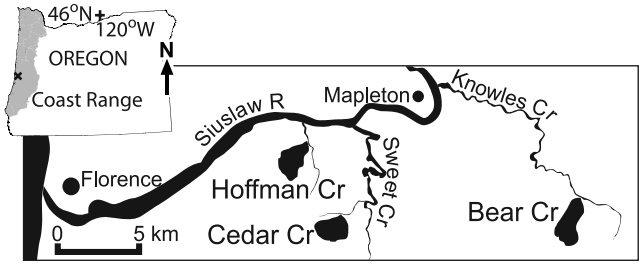

Figure 1. Map showing locations of Hoffman, Bear, and Cedar Creek study sites in the Oregon Coast Range.

bottoms and ridge tops are lowered at the same rate? Do these valleys evolve a morphology similar to that observed in the field? This paper will explore possible steady state valley morphologies, the mechanisms behind those morphologies, and the sensitivities of those morphologies to variations in the drivers of those mechanisms.

2. Field Sites in the Oregon Coast Range, United States

[10] Field work was sited in three drainage basins in the Oregon Coast Range: (1) a tributary to Cedar Creek ("Cedar Creek"), (2) a tributary to Hoffman Creek ("Hoffman Creek"), and (3) Bear Creek (Figure 1 and Table 1). These basins were chosen to satisfy several criteria: (1) they have similar lithologies; (2) they have similar drainage areas; (3) they have different shapes and, therefore, network structures that influence debris flow deposition in the mainstems; and (4) neither valley bottom nor midslope roads have affected debris flow runout and deposition in the mainstem valleys [*Swanson et al.*, 1977]. The basins are underlain by thick-bedded, shallowly dipping sandstone of the Eocene Tyee Formation except for the southernmost part of the Cedar Creek basin, which is underlain by intrusive volcanic rocks of an unnamed formation [*Peck*, 1961], which may have thermally altered and thus hardened nearby sandstone. Topography in the basins is steep and dissected by dense valley networks. Processes on the steep hillslopes (gradients of 0.84 are typical) are well described by stochastic soil production and nonlinear diffusion models [*Roering et al.*, 1999; *Heimsath et al.*, 2001]. Shallow, rapid landslides are commonly initiated in hillslope hollows during prolonged winter rainfall [*Montgomery et al.*, 2000], and the resulting debris flows likely dominate scour of parts of the drainage network with gradients above 0.03–0.10 [*Stock and Dietrich*, 2003; *Roering et al.*, 2005]. Soils are shallow (0–1.5 m [*Heimsath et al.*, 2001]) and have low bulk densities ($\sim$1 kg/m^3 [*Reneau and Dietrich*, 1991]).

[11] Diffusive hillslope transport processes, debris flows, and fluvial processes deliver sediment to the valley network [*Roering et al.*, 1999; *Lancaster and Casebeer*, 2007]. Valley bottom storage volumes in headwater valleys can be substantial: in Bear Creek, for example, *Lancaster and Casebeer* [2007] measured an average volume per down valley distance of 27 m^3/m with valleys typically 20 m wide and a volume per down valley distance as great as 190 m^3/m in a valley 44 m wide. Sediments stored on the valley bottom are typically evacuated over hundreds to thousands of years: the residence time of sediment in the Bear Creek valley (2.6 km length) is 1000 ^{14}C a [*Lancaster and Casebeer*, 2007].

[12] The landscape appears to represent a steady state between rock uplift and bedrock lowering [*Reneau and Dietrich*, 1991; *Heimsath et al.*, 2001]. Measurements of basin-scale denudation of $\sim 1 \times 10^{-4}$ m/a are similar in different parts of the Tyee Formation [*Bierman et al.*, 2001; *Heimsath et al.*, 2001], although hillslope-scale variations in lowering rate are substantial [*Heimsath et al.*, 2001]. Variations in rock uplift rate may also be substantial [*Personius*, 1995], and studies of longitudinal channel profiles and soil residence times have questioned whether these channels and their surrounding landscapes can be in steady state [*VanLaningham et al.*, 2006; *Almond et al.*, 2007]. Prevalent strath terraces [*Personius et al.*, 1993; *Personius*, 1995], which extend upstream to contributing areas as low as 5 km^2 and gradients as high as 0.05 downstream of the Cedar Creek site [*Underwood*, 2007], indicate that cross-sectional morphologies of these larger valleys do not represent steady states, but strath terraces are apparently absent at the smaller drainage areas of the study sites (Table 1). Also, while some valley bottom deposits in Bear Creek are thousands of years old, most sediment storage there is young and evacuated within 10^2–10^3 a [*Lancaster and Casebeer*, 2007]. It is likely, then, that these headwater valleys adjust quickly enough that their morphologies represent approximate steady states when conditions are averaged over such times, although transient states that do not record evidence of past morphologies cannot be ruled out.

3. Methods

3.1. Field Data and Observations

[13] Field data were collected to determine typical ranges of deposit depth and normalized valley width (ratio of valley to channel width) in valleys where debris flow deposits and debris dams are prevalent [see, e.g., *Lancaster et al.*, 2001, 2003; *May and Gresswell*, 2004; *Lancaster and Grant*, 2006; *Lancaster and Casebeer*, 2007], whether these quantities change systematically downstream and across the transition from dominance of scour by debris flows to fluvial dominance [see, e.g., *Stock and Dietrich*, 2003], and whether longitudinal channel profiles show any evidence of adjustment to episodic sediment supply. Observations were made to determine typical cross-sectional morphologies of such valleys.

[14] Quantitative, spatially referenced data from the field sites comprise the following: (1) longitudinal channel profiles; (2) active channel widths; (3) incised channel widths; (4) valley widths; and (5) valley cross sections; also, (6) channel substrates, i.e., bedrock versus alluvial channel beds, were mapped in the field; and (7) contributing areas along main channels were mapped from digital elevation models (DEMs). The mainstem channels were surveyed with hand level, stadia rod, and measuring tape from the basin outlets for 1–3 km (Table 1) to the upstream extent of observed debris flow deposits (although high waterfalls blocked further progress in Cedar Creek, so I cannot rule out the possibility of additional deposits upstream of the end of the survey). These distances were sufficient to encompass many tributary confluences, debris flow deposits, and debris dams [see, e.g., *Lancaster et al.*, 2001, 2003; *Lancaster and*

Table 2. Model Parameters, Values, and References

Parameter	Value or Distribution[a]	Reference
Soil production depth decay factor, a (m^{-1})	3.0	*Heimsath et al.* [2001]
Soil production rate at zero depth, ε_{hs0} (m/a)	2.68×10^{-4}	*Heimsath et al.* [2001]
Ratio of bedrock to soil density, ρ_r/ρ_s	2.0	*Heimsath et al.* [2001]
Nonlinear diffusivity, K_{hs} (m^2/a)	3.60×10^{-3}	*Roering et al.* [1999]
Critical slope for nonlinear diffusion, S_c	1.27	*Roering et al.* [1999]
Bedrock incision rate, K_b (m/a)	log-$U[10^{-3}, 10^{-1}]$	*Stock et al.* [2005]
Deposit incision rate, K_d (m/a)	log-$U[10^{-1}, 10^{0}]$	
Deposition probability, P_d (a^{-1})	log-$U[10^{-1.3}, 10^{-0.3}]$	
Mean deposition volume per unit distance, V (m^2)	log-$U[10^{0}, 10^{1}]$	
Transverse deposit slope standard deviation, σ_S	log-$N[10^{-2.3}, 10^{0.5}]$	
Deposit surface white noise amplitude, A_n (m)	0.01	
Channel width, b_c, and discretization, Δx (m)	2.0	
Time step, Δt (a)	1.0	
Ridge-to-ridge distance, l (m)	200	
Initial valley relief, Z_0 (m)	78	

[a]Log-$U[c_1, c_2]$ denotes a log-uniform distribution (i.e., the base 10 logarithms of the values are uniformly distributed) over the range from c_1 to c_2, inclusive; log-$N[c_1, c_2]$ denotes a lognormal distribution (i.e., the base 10 logarithms of the values are normally distributed) with a geometric mean and standard deviation of c_1 and c_2, respectively.

Grant, 2006; *Lancaster and Casebeer*, 2007]. Incised channel and valley width measurements and valley cross-section surveys were located to best characterize the sediment stored on the valley bottom, so the spacing of these cross sections varied but is on the order of 10^1–10^2 m [see *Lancaster et al.*, 2001; *Lancaster and Casebeer*, 2007]. Incised channel widths were measured between channel banks at about half the bank height, and valley widths were measured between the bases of steep (often oversteepened) valley sideslopes.

[15] The longitudinal surveys allowed interpolation beneath deposits between relative low points on the profile to provide calculated estimates of minimum depths to bedrock (each step with height greater than about 1 m was surveyed in detail [see *Lancaster and Grant*, 2006]). Bedrock is prevalent in the bed of Bear Creek, so interpolations between bedrock points provide good estimates of the actual depth to bedrock. Cross-sectional surveys and the sediment depth estimates yielded cross-sectional deposit areas, valley bottom widths, and thus average valley bottom deposit depths along the valleys [*Lancaster et al.*, 2001; *Lancaster and Casebeer*, 2007].

[16] Stream gradients were calculated from the surveyed profiles two different ways. First, for finding the apparent downstream limits of debris flow scour at all three sites, gradients were measured between points at elevation intervals of 10 m. These stream gradients were assigned to points and their contributing areas stream-wise equidistant from the calculation endpoints [e.g., *Snyder et al.*, 2000; *Stock and Dietrich*, 2003]. Second, for calculating a proxy for unit stream power (contributing area times stream gradient divided by active channel width, or AS/b_c) in Bear Creek, the local bedrock gradient was measured at each point on the survey from the interpolated and actual bedrock survey points. Gradients at each point were measured between the nearest upstream and downstream points on the survey. Active channel widths were measured between annual flow indicators (e.g., annual vegetation lines) at nearly every point on the surveyed longitudinal profile. These calculations were only done for Bear Creek, where estimates of bedrock elevation were good.

[17] Qualitative observations at the three field sites and other places within the Tyee Formation included (1) typical valley bottom bedrock morphologies and (2) typical morphologies of transitions between valley bottom and valley sideslope bedrock. Field data were collected and most observations were made in summer, 2000; qualitative observations have continued during other field work, particularly in 2003, 2006, and 2008.

3.2. Valley Cross-Section Model

[18] A new model simulates the evolution of valley cross-section morphology over geologic time (e.g., the time for exhumation of depths greater than the cross section relief from ridge to valley bottom). Bedrock is converted to regolith (''soil'') according to the depth-dependent soil production model of *Ahnert* [1987] and *Heimsath et al.* [2001]. Soil is transported along the cross section according to the nonlinear diffusion model of *Roering et al.* [1999] and similar to that posed by *Howard* [1994]. The present study employs the parameters published by *Heimsath et al.* [2001] and *Roering et al.* [1999] for the OCR (Table 2).

[19] An initially V-shaped valley cross section is inundated at random times according to a Bernoulli process [e.g., *Drake*, 1967] with random, exponentially distributed volumes of sediment that fill the valley from lowest to higher points to create a nearly flat, sediment-covered valley bottom and mimic debris flow deposition. I have frequently observed that channels tend to incise the debris flow deposits near the valley walls. Often these deposits are slightly tilted because of either superelevation of the flow around bends that becomes ''frozen'' upon deposition or the fact that the flows originated in a tributary and did not evenly deposit over the main stem valley. Fronts of debris flow deposits are also known to have rounded, snout-like fronts that are higher in the middle than on the sides [e.g., *Iverson*, 1997]. To mimic the tendency of debris flow deposits to push the channel to the sides because of either a slightly convex upward cross section or a tilt imposed by a valley bend or tributary junction, the deposit surface is given a small random tilt normally distributed about the horizontal. To allow the channel to incise somewhere other than the deposit margins and to mimic microtopography due to wood, boulders, and cobbles, small random perturbations are added to the sediment surface (Table 2), and the channel location is set to the lowest point in the valley.

[20] The channel incises by eroding sediment or bedrock at relatively fast and slow rates, respectively (Table 2). The rate of bedrock incision, while much slower than the rate of deposit incision, is still much greater than the maximum soil production rate (Table 2) and the denudation rate of 1×10^{-4} m/a commonly found for the Tyee Formation of the OCR [e.g., *Bierman et al.*, 2001; *Heimsath et al.*, 2001]. A large ratio of short-term incision rate to long-term denudation rate is consistent with *Stock et al.*'s [2005] finding in Washington and Taiwan and is consistent with steady state in a temporally averaged sense: if bedrock is often shielded by sediment or the channel does not span the entire valley bottom, then instantaneous bedrock incision rates must be greater than the long-term lowering rate in order to maintain that rate averaged over times that are long relative to the period between times that the bedrock is exposed in the channel bed. The actual values of the bedrock and deposit incision rates are poorly constrained and therefore part of the focus of the sensitivity analysis explained below.

[21] Soil production and nonlinear diffusion are applied to the valley bottom as well as the valley sides, but deposition by these processes is disallowed at the channel point, i.e., the channel is assumed able to immediately evacuate any sediment provided by these processes (but not debris flow deposition). The channel position is therefore fixed until the next stochastic deposition event, when the channel position is reset as described above.

[22] The boundaries on each end of the cross section are cyclical such that gradients are calculated between domain ends separated by a single horizontal distance increment (equal to the channel width) and material removed from one side by nonlinear diffusion is delivered to the other side. Each simulation proceeded until the bedrock of the valley bottom had been lowered a distance equal to twice the initial relief of the cross section (Table 2). For cases where steady state was possible (i.e., average valley bottom lowering rate not greater than the maximum soil production rate), the simulations proceeded until the bedrock of the ridge top had also lowered a distance equal to twice the initial relief. For the purposes of calculating average quantities such as valley bottom width, average sediment depth, valley bottom lowering rate, and toe slope height, values were averaged over the final amount of lowering equal to one-third of the initial relief (Table 2). Averages taken every 1 ka (equal to 1000 time steps) tracked those quantities over time.

3.3. Model Sensitivity Analysis

[23] The parameter space of this model is potentially large and multidimensional, and the model output is itself multidimensional, but dimensional analysis and consideration of parameters likely to be interesting can shrink the number of dimensions in the parameter space to a reasonable number. Model outputs are a function of the parameters as follows:

$$(Z, Z_{ts}, w, H_v, H_{hs}, \varepsilon_v, \varepsilon_{hs}) = F(K_b, K_d, \varepsilon_{hs0}, K_{hs}, a, S_c, V, P_d, A_n, \sigma_S, b_c, l, \rho_r, \rho_s), \quad (1)$$

where Z is the total bedrock relief (L); Z_{ts} is the toe slope height (L), defined as the average elevation difference between valley bottom margin and next higher points; w is the valley bottom width (L), defined as the horizontal distance between points where hillslope gradient first decreases by more than 10% (an arbitrary value based on inspection of simulated cross sections); H_v is the average valley bottom deposit thickness (L); H_{hs} is the average hillslope soil depth (L); ε_v is the average valley bottom bedrock lowering rate (L/T); ε_{hs} is the ridge top bedrock lowering rate (L/T); K_b is the instantaneous bedrock incision rate (L/T); K_d is the deposit incision rate (L/T); ε_{hs0} is the maximum bedrock lowering rate by soil production, i.e., at zero soil thickness (L/T); K_{hs} is the nonlinear diffusion constant (L^2/T); a is the soil production exponential decay scale (L^{-1}), i.e., the inverse of the soil depth at which the hillslope lowering rate, ε_{hs}, is reduced to 1/e of its maximum value, ε_{hs0}; S_c is the gradient at which the hillslope soil transport becomes infinite [*Roering et al.*, 1999]; V is the mean deposit volume per unit valley length (L^2), and for exponentially distributed volumes, the mean is equal to the standard deviation; P_d is the probability of episodic deposition at each time step (T^{-1}), i.e., the deposition event frequency; A_n is the amplitude of white noise added to the deposit surface (L); σ_S is the standard deviation of the transverse slope of the deposit surface; b_c is the channel width, equal to the discretization (L); l is the simulation domain width (L), i.e., the ridge-to-ridge distance; and ρ_r and ρ_s are the rock and soil bulk densities, respectively (M/L^2). Two of the parameters, S_c and σ_S, are dimensionless and do not enter the dimensional analysis in the sense that they do not affect the number of dimensionless numbers required to characterize the problem, although dimensionless parameters may be included in other dimensionless numbers.

[24] For the 19 remaining output variables and parameters with 3 fundamental units, the Buckingham Π theorem states that the system is described by $19 - 3 = 16$ independent dimensionless numbers [*Buckingham*, 1915]. Characteristic length scales are $1/a$ and V/b_c for hillslope and valley bottom processes, respectively. Characteristic times are $1/(\varepsilon_{hs0}a)$ and $1/P_d$ for hillslope and valley bottom processes, respectively. From standard dimensional analysis [*Bridgman*, 1922], the nondimensional form of equation (1) is

$$\left(\frac{Zb_c}{V}, \frac{Z_{ts}b_c}{V}, \frac{wb_c}{V}, \frac{H_v b_c}{V}, \frac{\varepsilon_v b_c}{VP_d}, H_{hs}a, \frac{\varepsilon_{hs}b_c}{VP_d}\right) = F\left(\frac{K_b}{K_d}, \frac{K_d b_c}{VP_d}, \frac{K_{hs}a}{\varepsilon_{hs0}}, \frac{lb_c}{V}, \frac{A_n}{\sigma_S b_c}, \frac{\rho_s}{\rho_r}, \frac{K_b}{\varepsilon_{hs0}}, \frac{b_c}{Va}, \frac{b_c^2}{V}\right). \quad (2)$$

These dimensionless numbers include those that are simply scaled by the quantity representing the relevant fundamental unit and others that represent interactions among processes.

[25] All of the dimensionless ratios on the right-hand side of equation (2) will affect the model results, but some may be eliminated from a sensitivity analysis. The ratio, $K_{hs}a/\varepsilon_{hs0}$, represents the ratio of soil transport to soil supply by weathering, and its magnitude determines whether the slope will be covered with soil; I eliminate this number from further analysis because this study primarily addresses the morphology of the valley bottom. The ratio, lb_c/V, describes the size of the simulation domain relative to mean deposition volume and therefore simply limits the largest valleys that can be produced in the simulation, and this ratio is

Table 3. Constraints on Parameters Based on Targeted Conditions in Simulations

Condition Type	Target Condition	Parameter Constraint
Significant incision rate	$\varepsilon_v \geq 10^{-6}$ m/a	$N_D \leq 3.0$
Steady state cross section	$0.95\ \varepsilon_v \leq \varepsilon_{hs} \leq 1.05\varepsilon_v$	$N_D \geq \log N_I + 1.5$

eliminated from further analysis. The density ratio, ρ_s/ρ_r, is also eliminated because it primarily affects the hillslope soil. The model premise essentially includes the condition that $K_b/\varepsilon_{hs0} \gg 1$. Although the results are still potentially sensitive to this ratio, the value of ε_{hs0} is kept fixed to the average value determined by *Roering et al.* [1999], and I eliminate the ratio from the sensitivity analysis. The ratio, $b_c/(Va)$, describes the susceptibility of the valley bottom to physical weathering and is eliminated because, for values of this ratio less than unity or $K_b > \varepsilon_{hs0}$, both of which are usually true, valley bottom lowering will be insensitive to this ratio. Finally, the ratio, b_c^2/V, which describes the size of the channel relative to the mean deposit volume, should be near unity for the purposes of examining the effects of depositional events that inundate the channel and lead to avulsion and is therefore eliminated. Thus, all but three of the dimensionless ratios on the right-hand side of equation (2) are eliminated by inspection from the sensitivity analysis.

[26] The remaining dimensionless ratios form the potential parameter space for investigation. First, the ratio of bedrock and deposit incision rates is the incision number

$$N_I = \frac{K_b}{K_d}. \tag{3}$$

Second, the deposition number, N_D, describes the deposition rate relative to the rate of deposit evacuation

$$N_D = \frac{VP_d}{K_d b_c}. \tag{4}$$

Third, the transverse slope number, N_{TS}, describes the relief of the deposit surface due to the imposed transverse slope relative to the relief imposed by random noise

$$N_{TS} = \frac{\sigma_S b_c}{A_n}. \tag{5}$$

Note that one of the parameters, σ_S, that was already dimensionless has been included in this number.

[27] Simulations addressed the sensitivity of the valley morphology to N_I, N_D, and to a lesser extent, N_{TS}, by fixing some parameters (particularly those not included in N_I or N_D) and choosing values of the other parameters from probability distributions for each one of the hundreds of simulations (Table 2). One round of simulations ($N = 200$) established reasonable bounds for N_{TS} (Table 2). A second round of simulations ($N = 702$) established bounds on N_I and N_D for steady state solutions at reasonable incision rates (Table 3). A final round of simulations ($N = 910$) explored the model sensitivity to N_I and N_D (results were relatively insensitive to N_{TS}). Distributions for K_b, K_d, V, and P_d were chosen to represent broad but reasonable parameter ranges spanning an order of magnitude or more. In part, parameter values were considered reasonable if they produced stable model solutions, but the ranges are somewhat arbitrary.

4. Results

4.1. Field Data

[28] The surveyed streams all span a break in concavity [see, e.g., *Flint*, 1974; *Snyder et al.*, 2000] that is identified according the method of *Stock and Dietrich* [2003] (Table 1 and Figure 2). *Stock and Dietrich* [2003] attributed such breaks to the transition between dominance of bedrock erosion by debris flows and fluvial processes. Debris flow deposits are prevalent in all 3 sites, and the surveyed profiles included 18 debris dams with heights $\geq$2 m [*Lancaster and Grant*, 2006].

[29] The field sites' valleys are several times wider than the channels, reach-averaged deposit depths fall in the approximate range 1–2 m (Table 1), and the sites with greater ratios of valley width to channel depth (normalized valley width) also have greater deposit depths. Variations of normalized valley widths and sediment depths with contributing area are not generally significant over the whole range of contributing area. Normalized widths and deposit depths generally have different trends above and below the inflection points in stream gradients (i.e., the breaks in power law scaling), but the differences are not consistent among the sites, and many of the fits are not significant at the 5% level (Figure 2). Better access at Hoffman Creek allowed measurements further upstream to smaller valleys and contributing areas than at the other sites. At Hoffman and Bear Creeks, substantial parts of the surveyed reaches' upstream ends were recently scoured by debris flows. At Cedar Creek, the valley just upstream of the surveyed reach was recently scoured by a debris flow. It is likely that frequency of debris flow deposition increases downstream through the upper reaches, but such trends may be absent in the lower reaches.

[30] These data show that valley bottom widths and average sediment depths are not easily described with simple relationships predicting greater deposition and accommodation space downstream. Rather, local variations in the likelihood of debris flow deposition (e.g., at tributary junctions [e.g., *Lancaster et al.*, 2001; *Lancaster and Casebeer*, 2007]) contribute to great variance in normalized valley bottom widths and average sediment depths. Note that debris flow deposits are common in all the study sites, both above and below the inflections in gradient [*Swanson et al.*, 1977; *Lancaster et al.*, 2001; *May and Gresswell*, 2003, 2004; *Lancaster and Grant*, 2006; *Lancaster and Casebeer*, 2007].

[31] The correspondence between sediment storage (surveyed cross-sectional area of valley bottom deposits) and a proxy for unit stream power, AS/b_c, is not particularly good in the sense of a statistical correlation, but the data indicate that, at least in some places, sediment storage maxima correspond to maxima in unit stream power (Figure 3).

[32] Observations of the bedrock surface of the valley bottom were abundant only at the Bear Creek site, where recent debris flows have scoured long reaches in the upstream half of the surveyed profile, and incision by the stream has revealed much of the bedrock in the lower half [*Lancaster and Casebeer*, 2007]. For the entire surveyed

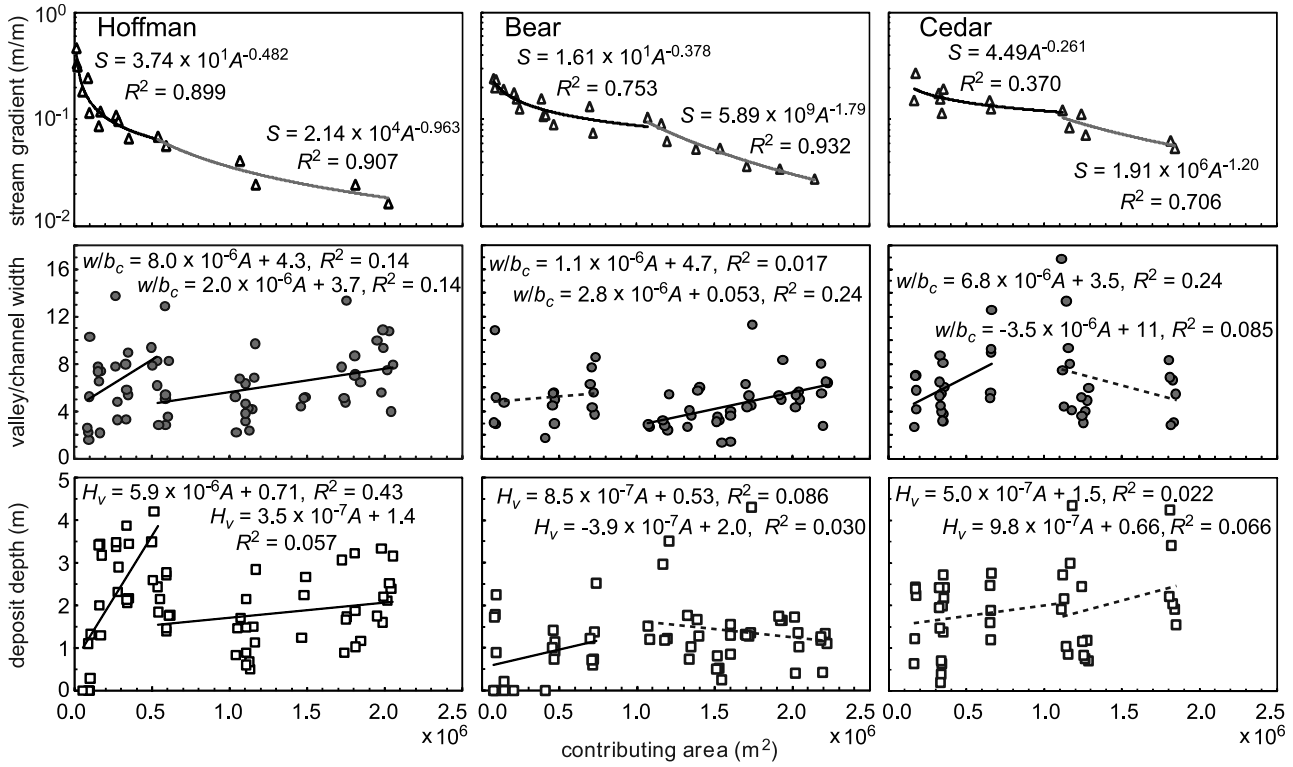

Figure 2. Results from Hoffman, Bear, and Cedar Creek sites. (top) Stream gradient (slope) versus contributing area and power law fits above and below apparent breaks in concavity (negative of exponent of power law fit) identified by successive pruning of the minimum contributing area until concavity reaches a maximum [*Stock and Dietrich*, 2003] (see Table 1). (middle) Ratio of valley bottom width (measured on deposit surfaces) to incised channel width, w/b_c, versus contributing area and linear fits. (bottom) Average valley bottom deposit depth (deposit cross-sectional area divided by width), H_v, versus contributing area and linear fits. Equations of all fits are shown, where S is slope, w is valley width (m), b_c is channel width (m), H_v is deposit depth (m), and A is contributing area (m^2), and each fit with its R^2 or fraction of variance explained. Slope-area fits are highly significant (significance levels, $\alpha \ll 5\%$). Fits to w/b_c and H_v are not generally significant; fits that are not significant at the 5% level are shown with dashed lines.

length of Bear Creek, observed bedrock bottoms of valley cross sections are flat, i.e., the bottoms are approximately horizontal in cross section with only microtopography, grooves, and potholes with relief on the order of 10^{-1} m, although bedrock steps are often irregular and not perpendicular to the downstream direction (Figure 4). My observations elsewhere in the OCR's Tyee indicate that such flat valley bottoms are prevalent where bedrock valley floors can be observed. Bear Creek flows into Knowles Creek where, upstream of the Bear Creek confluence, I observed a reach 50–100 m in length to be nearly devoid of sediment and to have a flat bedrock valley bottom with abrupt transitions to oversteepened toe slopes on either side of the valley bottom. At the confluence of the Cedar Creek site with its mainstem, bedrock incision by the main stem has revealed part of the flat tributary valley bedrock, its overlying sediment, and an abrupt transition to a steep valley side in cross section. Upstream of the surveyed Cedar Creek reach, I observed valley bottoms nearly devoid of sediment and nearly flat in cross section, similar to the upstream end of the Bear Creek reach. These wide, flat valley bottoms do, in almost all cases that I have observed, give way upstream to more curved bedrock shapes where I

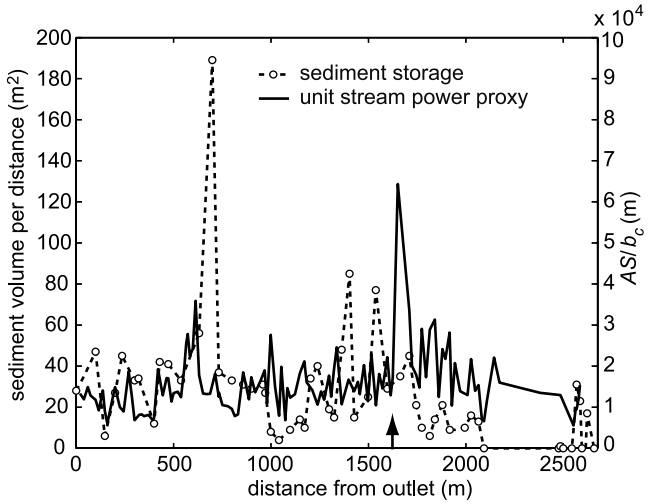

Figure 3. Sediment storage (volume per unit distance) and unit stream power proxy (contributing area times bedrock gradient divided by active channel width) versus distance from the outlet for Bear Creek. Vertical arrow near bottom shows the location of the slope-area inflection [*Stock and Dietrich*, 2003] (Table 1 and Figure 2).

Figure 4. View upstream of flat (approximately horizontal in cross section) bedrock valley bottom exposed by recent debris flow scour in Bear Creek at 1820 m from the outlet. Note subtle grooves and other microtopography in the foreground as well as bedrock steps that are not perpendicular to the downstream direction. Author shown in the middle of the image for scale. Photo by S. K. Hayes in 2000.

infer that debris flow deposition is relatively rare. Such a transition is evident, for example, at the upstream end of the surveyed reach of the Hoffman Creek site, in the steep decline in valley widths with decreasing contributing areas $<2 \times 10^5$ m^2.

4.2. Valley Cross-Section Simulations

[33] Preliminary sensitivity analysis ($N = 200$) found only modest sensitivity, primarily of valley bottom width, to $N_{TS} \sim 10^{-1}$–10^{1}, its approximate range in subsequent simulations (Table 2). Next, simulations ($N = 702$) varied K_b, K_d, V, P_d, and σ_S (see Table 2) to establish constraints on N_D for steady state solutions (Table 3; the complete ranges of N_I and N_{TS} produced steady state solutions). Simulated incision rates had a large gap in values $<10^{-6}$ m/a; incision rates lower than this value were much lower, e.g., $<10^{-50}$ m/a; these simulations were excluded from analysis (Table 3). I inferred that cross sections had reached steady state for simulations with equal ridge top and valley bottom lowering rates (plus or minus 5%; see Table 3). Finally, simulations ($N = 910$) again varied the above parameters as in Table 2 but also imposed the constraints of Table 3. Of these simulations, 22% ($N = 202$) met the steady state and lowering rate criteria (Table 3), and this latter subset formed the "steady state" simulations.

[34] Steady state solutions were found over the entire range of each input parameter, K_b, K_d, V, P_d, and σ_S, and of the incision number, N_I, but only over a restricted range of deposition number, N_D (Table 2 and Figure 5). The minimum N_D for steady state increases with greater N_I: for $N_I > 10^{-2}$, all steady state solutions had $N_D > 1$. Ranges of model outputs produced by the steady state solutions are given in Table 4.

[35] Simulated valley cross-section morphologies at steady state range from flat valley bottoms and greatly oversteepened toe slopes higher than average deposit thicknesses to more curved valley bottoms with average deposit thicknesses greater than heights of toe slopes, which may lack significant oversteepening (Figure 6 and Table 5). Cross sections with oversteepened toe slopes are typical of valleys in the field sites and elsewhere in the OCR's Tyee Formation, especially toward headward ends of valley networks, toe slopes are often high and steep enough to make field workers' entry to and egress from these valleys difficult and sometimes hazardous.

[36] Valley bottom lowering rates are highly variable over time but, on average, quickly approach their steady state values (Figure 6). Because the initial ridge top shape is pointed (the inverse of the initial "V" of the valley bottom), ridge top lowering rates begin near their maximum rates (i.e., ε_{hs0}, the maximum soil production rate) but quickly fall to about 7×10^{-5} m/a as ridge tops become rounded. As the effect of valley bottom lowering propagates upslope, ridge top lowering rates rebound, typically overshoot, and finally settle back down to their steady state rates. With greater steady state lowering rates (Figures 6a and 6b), the valleys often migrate laterally, and these lateral movements appear as increases in toe slope height that initiate increases in ridge top lowering rates until toe slope heights drop back down to approach average deposit thicknesses, at which time ridge top lowering rates abruptly drop. The simulations with greater lowering rates have toe slope heights greater on average than average deposit thicknesses (Figures 6a and 6b and Table 5), whereas simulations with smaller lowering rates have toe slope heights smaller on average than average deposit thicknesses (Figures 6c and 6d and Table 5). Simulations with greater deposition number, N_D, have greater valley widths, regardless of incision rate. Over time, greater valley bottom widths typically coincide with greater average deposit thicknesses and smaller valley bottom lowering rates. Changes in valley bottom width are stepwise because they occur in increments of channel width, b_c, equal

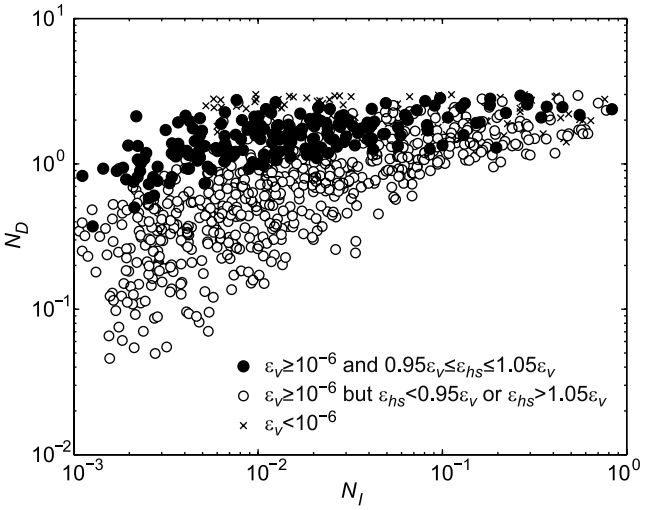

Figure 5. Constrained set of 910 simulations in parameter space of N_I and N_D. Solid black circles show simulations meeting both target conditions in Table 3, significant incision rate and steady state cross section ($N = 202$). Open circles show simulations meeting only the significant incision rate condition ($N = 619$). Simulations with insignificant incision rates are marked with crosses ($N = 89$).

Table 4. Ranges of Parameters and Time-Averaged Outputs for All Steady State Simulations and Those Within a Restricted Range of Lowering Rates[a]

Parameter or Output	Steady State	OCR Lowering Rates
Incision number, N_I	1.11×10^{-3}–0.832	1.27×10^{-3}–0.448
Deposition number, N_D	0.372–2.94	0.372–2.94
Transverse slope number, N_{TS}	0.0908–15.1	0.149–13.1
Valley bottom width, w (m)	7.65–189	7.65–79.4
Average deposit depth, H_v (m)	1.86–15.6	1.86–8.43
Valley lowering rate, ε_v (m/a)	1.31×10^{-6}–2.72×10^{-4}	7.0×10^{-5}–1.4×10^{-4}
Toe slope height, Z_{ts} (m)	0.305–23.2	1.68–6.82
Total bedrock relief, Z (m)	13.4–132	59.9–94.2

[a]Restricted range of lowering rates is $7.0 \times 10^{-5} \leq \varepsilon_v \leq 1.4 \times 10^{-4}$ m/a, similar to those found for the Tyee Formation of the Oregon Coast Range [*Reneau and Dietrich*, 1991; *Bierman et al.*, 2001; *Heimsath et al.*, 2001].

to the horizontal discretization (Table 2). The minimum possible valley width is the channel width. The initial valley bottom width, equal to the domain width, l, is a failure of the criterion for identifying the valley bottom.

4.3. Model Sensitivities and Interdependencies at Steady State

[37] Multivariate power law fits to the outputs of the steady state simulations indicate the relative sensitivities of model behavior to the incision and deposition numbers, N_I and N_D, respectively (Figure 7). Fits to valley bottom width, w, and average deposit depth, H_v, take the following forms:

$$w = (16.0)\left(N_I^{-0.0762}\right)\left(N_D^{1.37}\right) \equiv F_w, \tag{6}$$

$$H_v = (3.85)\left(N_I^{0.0507}\right)\left(N_D^{0.765}\right) \equiv F_H. \tag{7}$$

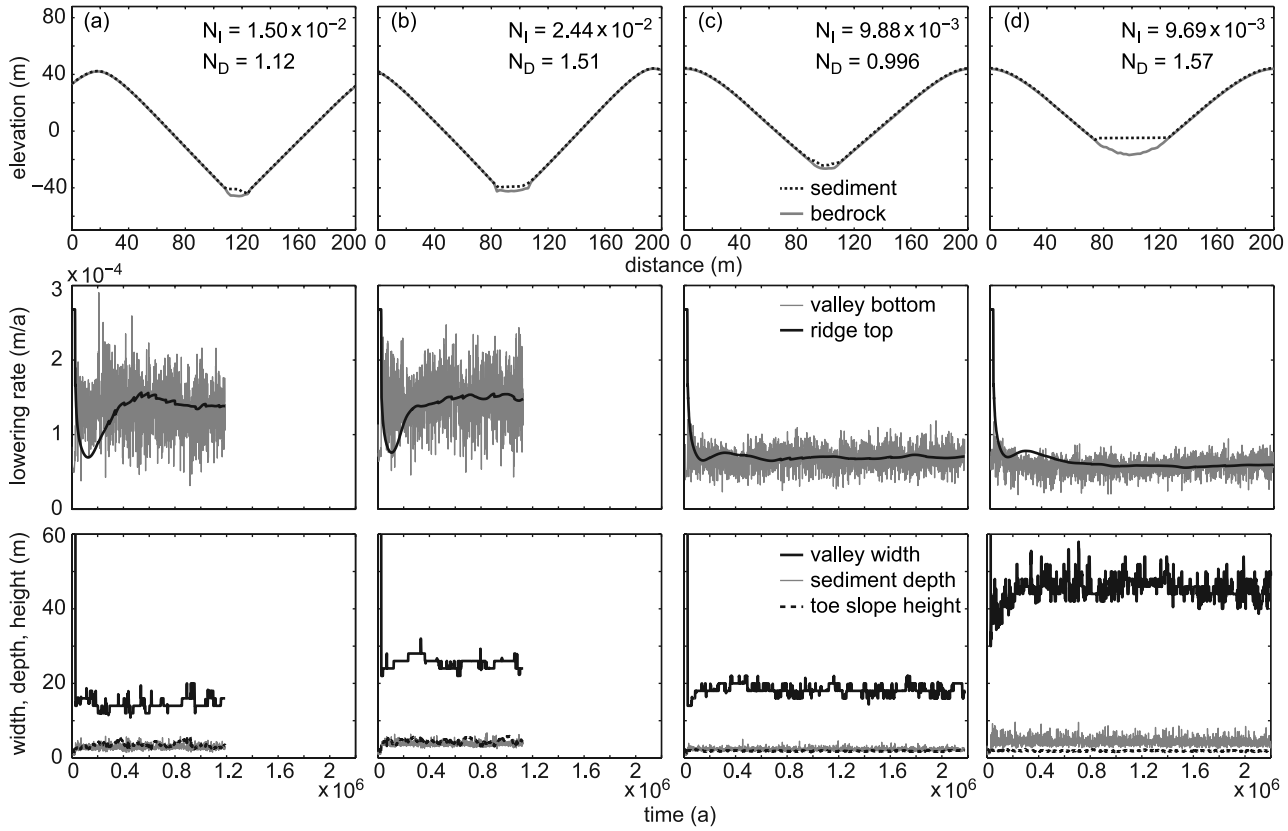

Figure 6. (top) Examples of steady state simulated valley cross sections at ends of simulations. (middle) Corresponding valley bottom and ridge top lowering rates versus time. (bottom) Corresponding valley bottom widths, average sediment depths, and toe slope heights versus time. Each point in time-varying quantities represents an average over 1 ka. Column (a) is for large N_I and small N_D, column (b) is for large N_I and large N_D, column (c) is for small N_I and small N_D, and column (d) is for small N_I and large N_D. Parameter and response variable values are shown in Table 5.

Table 5. Parameters and Time-Averaged Outputs for Examples of Simulated Steady State Valleys[a]

Simulation	K_b (m/a)	K_d (m/a)	V (m^2)	P_d (a^{-1})	N_I	N_D	N_{TS}	Width (m)	Sediment Depth (m)	Toe Slope Height (m)	Valley Lowering Rate (m/a)
Figure 6a	2.86×10^{-3}	0.191	3.35	0.128	1.50×10^{-2}	1.12	6.00	15.3	2.90	3.10	1.32×10^{-4}
Figure 6b	1.27×10^{-2}	0.520	3.46	0.453	2.44×10^{-2}	1.51	5.44	25.4	3.77	4.68	1.45×10^{-4}
Figure 6c	2.56×10^{-3}	0.259	1.39	0.371	9.88×10^{-3}	0.996	1.13	18.8	2.32	1.88	7.00×10^{-5}
Figure 6d	2.77×10^{-3}	0.286	9.59	0.0935	9.69×10^{-3}	1.57	1.03	46.0	4.31	1.95	5.96×10^{-5}

[a]Actual time of averaging depends on the lowering rate, i.e., outputs are averaged over the time for lowering equal to one-third of the initial relief or 26 m (Table 2).

The valley bottom lowering rate is normalized by the maximum possible incision rate. The fit to ε_v/K_b is

$$\frac{\varepsilon_v}{K_b} = \left(9.69 \times 10^{-3}\right)\left(N_I^{-0.236}\right)\left(N_D^{-2.17}\right) \equiv F_E. \quad (8)$$

Finally, valley bottom capacity is defined as the product of toe slope height and valley bottom width, and it is normalized by mean deposit volume per unit downstream length. The fit to $Z_{ts}w/V$ is

$$\frac{Z_{ts}w}{V} = \left(1.30 \times 10^{2}\right)\left(N_I^{0.446}\right)\left(N_D^{-0.3639}\right) \equiv F_V. \quad (9)$$

[38] Within the parameter space defined by the steady state simulations, valley bottom width, average deposit depth, and normalized incision rate are most sensitive to deposition number, N_D, and normalized valley capacity to incision number, N_I. Note, however, that the range of N_D is much smaller than the range of N_I. Deposition number, therefore, only appears dominant in the contour plots (Figure 7) if the magnitude of N_D's exponent is much larger than the magnitude of N_I's, as is the case in equations (6)–(8). Conversely, in equation (9) the exponents have similar magnitudes, and N_I appears to dominate the sensitivity of normalized valley capacity (Figure 7g).

[39] Sensitivities of the steady state simulation outputs vary widely. Average deposit depths at steady state vary over 1 order of magnitude (less than 1 order but for one point) and valley bottom widths and normalized valley capacities vary over slightly more than 1 order of magnitude. In contrast, steady state normalized bedrock lowering rates vary over 3 orders of magnitude over the sampled parameter space. This contrast is evident in the power law fit of normalized bedrock lowering rate to valley bottom width and average deposit depth for the steady state simulations (Figure 8a)

$$\frac{\varepsilon_v}{K_b} = (3.20)\left(w^{-0.739}\right)\left(H_v^{-2.07}\right) \equiv F_{wH}. \quad (10)$$

This relationship shows that normalized bedrock lowering rate is especially sensitive to average deposit depth.

[40] Another interaction between average deposit depth and incision rate is evident from a power law relationship between the ratio of toe slope height to average deposit depth, Z_{ts}/H_v, and the ratio of valley bottom lowering rate and maximum soil production rate, $\varepsilon_v/\varepsilon_{hs0}$, for the steady state simulations (Figure 8b)

$$\frac{Z_{ts}}{H_v} = (1.49)\left(\frac{\varepsilon_v}{\varepsilon_{hs0}}\right)^{0.618}. \quad (11)$$

For valley bottom lowering rates greater than half the maximum soil production rate ($\varepsilon_v/\varepsilon_{hs0} > 0.5$), toe slope heights are typically greater than average deposit depths ($Z_{ts}/H_v > 1$). As the valley bottom lowering rate approaches the maximum soil production rate ($\varepsilon_v/\varepsilon_{hs0} \rightarrow 1$), the ratio, Z_{ts}/H_v, increases faster than the trend for the other steady state points.

4.4. Model Sensitivities and Interdependencies Beyond Steady State

[41] The nonsteady state simulation results (Figures 7 and 8), appear to elaborate on the steady state trends for valley bottom width, normalized bedrock lowering rate, and the ratio of toe slope height and average deposit depth, but the nonsteady state points appear to parallel the steady state trends for average deposit depth and normalized valley capacity. Whereas many nonsteady state points simply fell outside the bounds of the criterion for steady state (Table 3) and therefore fall among the steady state points on the plots, the main locus of nonsteady state points is at valley incision rates greater than the maximum soil production rate

Figure 7. Sensitivity of output variables (a and b) valley bottom width, w; (c and d) average deposit depth, H_v; (e and f) normalized incision rate, ε_v/K_b; and (g and h) normalized valley capacity, $Z_{ts}w/V$, to incision number, N_I, and deposition number, N_D. (a, c, e, and g) Planes defined by multivariate power law fits (equations (6)–(9)) are contoured and shown with locations of steady state simulations (meeting both target conditions in Table 3; $N = 202$) in N_I–N_D space. Deposition rates relative to potential evacuation rates increase toward the tops of the graphs, and instantaneous bedrock incision rates relative to deposit incision rates increase toward the right sides of the graphs (equations (3) and (4)). (b, d, f, and h) Deviations from fits (equations (6)–(9)) are shown by projecting model results onto planes with horizontal axes defined by equations (6)–(9), functions of N_I and N_D, and vertical axes defined by actual values of output variables. Fits are solid lines of 1:1 correspondence plus and minus standard (root-mean square) errors (dashed lines). Nonsteady state points (meeting the significant incision rate condition in Table 3; $N = 619$), which were not used in fitting power laws (equations (6)–(9)) are also shown. In Figure 7b, N_I decreases and N_D increases with increasing F_w (equation (6)). In Figure 7d, both N_I and N_D increase with increasing F_H (equation (7)). In Figure 7f, N_I and N_D both decrease with increasing F_E (equation (8)). In Figure 7h, N_I increases and N_D decreases with increasing F_V (equation (9)).

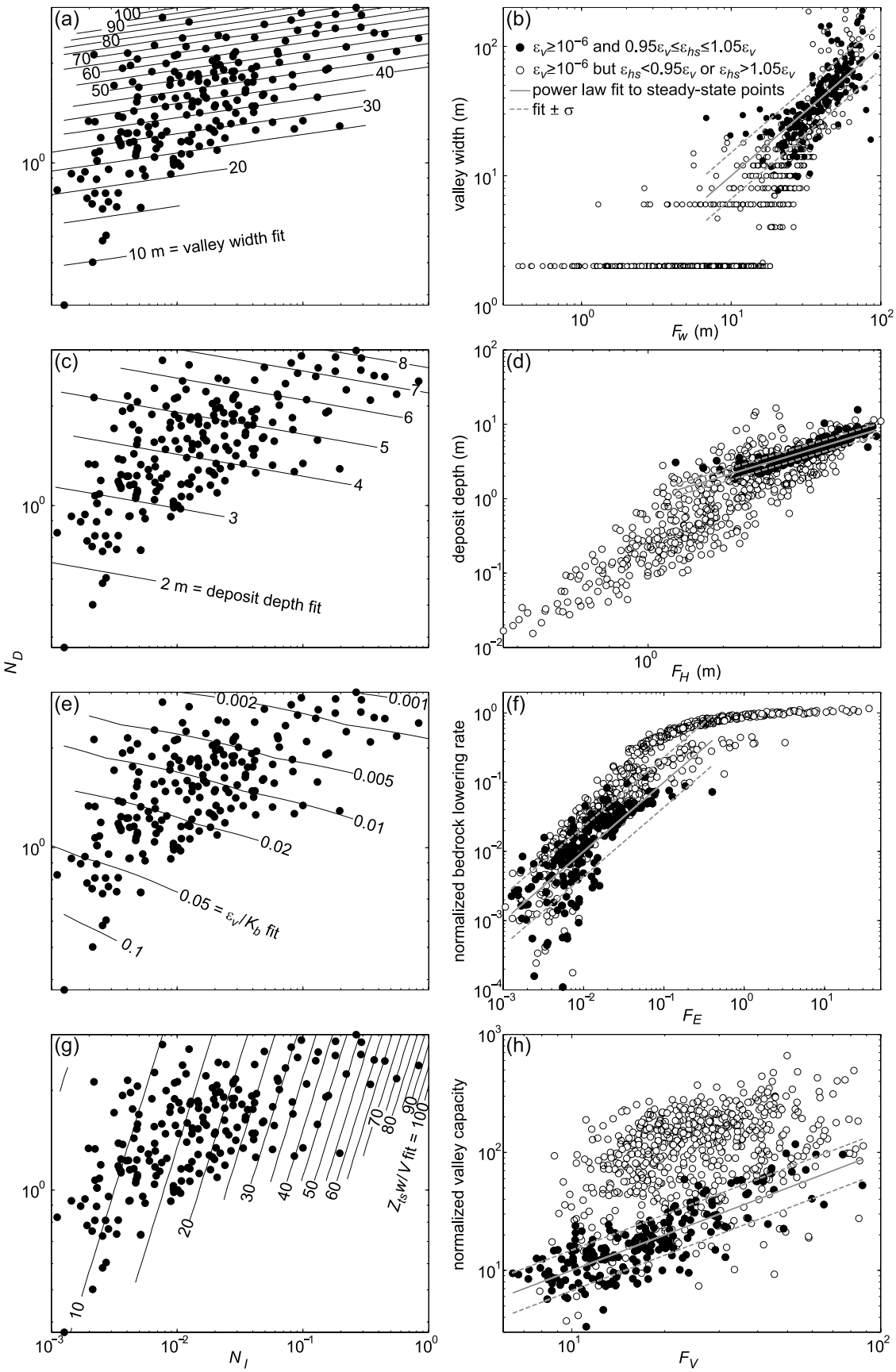
(a)
100
90
80
70
60
50
40
30
20
10 m = valley width fit
(b)
$\varepsilon_v \geq 10^{-6}$ and $0.95\varepsilon_v \leq \varepsilon_{hs} \leq 1.05\varepsilon_v$
$\varepsilon_v \geq 10^{-6}$ but $\varepsilon_{hs} < 0.95\varepsilon_v$ or $\varepsilon_{hs} > 1.05\varepsilon_v$
power law fit to steady-state points
fit ± σ
valley width (m)
F_w (m)
(c)
8
7
6
5
4
3
2 m = deposit depth fit
N_D
(d)
deposit depth (m)
F_H (m)
(e)
0.002
0.001
0.005
0.01
0.02
0.05 = ε_v/K_b fit
0.1
(f)
normalized bedrock lowering rate
F_E
(g)
10
20
30
40
50
60
70
80
90
100 = $Z_{ts}w/V$ fit
N_I
(h)
normalized valley capacity
F_V

Figure 7

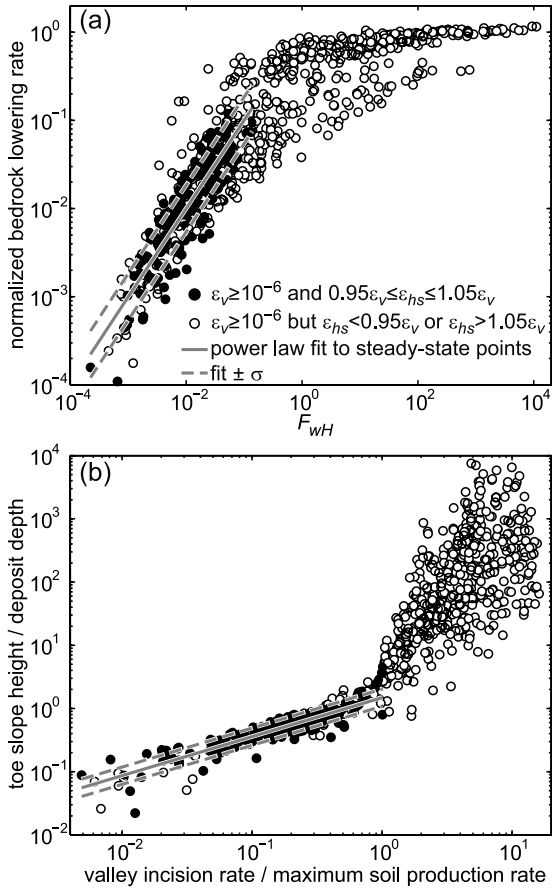

Figure 8. Relationships among output variables and fits with standard errors. (a) Normalized incision rate, ε_v/K_b, versus multivariate power law, F_{wH}, of valley bottom width, w, and average deposit depth, H (equation (10)). (b) Ratio of toe slope height to average deposit depth, Z_{ts}/H, versus ratio of valley incision rate and maximum soil production rate, $\varepsilon_v/\varepsilon_{hs0}$ and power law fit (equation (11)). In both Figures 8a and 8b, fits are to steady state simulations only (solid circles, $N = 202$; Table 3), but simulations only meeting the significant incision rate condition are also shown (open circles, $N = 619$; Table 3); lines of 1:1 agreement are shown with lines showing standard errors.

($\varepsilon_v/\varepsilon_{hs0} > 1$; Figure 8b) and normalized bedrock lowering rates, $\varepsilon_v/K_b > 10^{-1}$ (Figures 7f and Figure 8a). At these high incision rates, small N_D values indicate that potential evacuation substantially exceeds deposition (Figure 5), valley bottom widths and average deposit depths become small (Figures 7b and 7d), and normalized bedrock lowering rates approach unity. The maximum possible normalized bedrock lowering rate is slightly larger than unity because of soil production on valley floors with small deposit thicknesses. The appearance of subparallel clusters is due to the discretization; the tightest clusters at the highest incision rates all have valley widths equal to the channel width.

4.5. Controls on Model Output Ranges and Comparison to Field Data

[42] The ranges of output values at steady state (Table 4) are limited by the size of the model domain and the maximum soil production rate. Valley width and sediment depth are covariant in the simulations, so to some degree the maximum deposit depth is limited by the maximum valley width, which is in turn limited by the width of the simulation domain, l. Similarly, since the valley lowering rate is also dependent on valley width and sediment depth (e.g., Figure 8a), the minimum "significant" lowering rate is also limited by l. Total bedrock relief, Z, and toe slope height, Z_{ts}, are both highly correlated with lowering rate (e.g., Figure 8b), so the minimum relief is also limited by l. Limits at opposite extremes of steady state outputs are generally limited by the maximum soil production rate, ε_{hs0}. At steady state, the valley lowering rate can be no larger than the maximum soil production rate, so the maximum values of relief and toe slope height are also limited by ε_{hs0}. Likewise, since incision rate is so highly dependent on valley bottom width and sediment depth, the minima of the latter two at steady state are also limited by ε_{hs0}.

[43] Because of their dependence on an arbitrary parameter choice, the maximum valley width and deposit depth are not directly comparable with field data. The minimum valley width and deposit depth are dependent on a parameter derived from data from the OCR's Tyee Formation [*Roering et al.*, 1999] and may therefore be compared to the field data if the comparison simulations are restricted to those with lowering rates within the range of those found in similar OCR sites [*Reneau and Dietrich*, 1991; *Bierman et al.*, 2001; *Heimsath et al.*, 2001] (Table 4). The restricted minimum valley width corresponds to a valley width-to-channel width ratio of 3.83, which is relatively low but within one standard deviation of the mean ratio for all three field sites. The minimum steady state deposit depth falls between the means for Cedar and Hoffman Creeks and is higher than, but within one standard deviation of, the mean deposit depth for Bear Creek. The restricted maxima are both greater than the greatest values observed: the restricted maximum width corresponds to a valley width-to-channel width ratio of 39.7, more than two standard deviations higher than any of the mean ratios at the field sites. Similarly, the restricted maximum average sediment depth is greater than any measured in the field.

5. Discussion

[44] The simple model presented here reproduces important aspects of real valleys in the field sites in the Oregon Coast Range, and the results elucidate valley incision processes, steady state in systems with stochastic forcing, and adjustments of bedrock valleys and channels. The simulated valley bottoms display a range of morphologies, including some that are not as flat as I surmise most OCR valleys to be, and output values of valley bottom width and average sediment depth span a greater range than the field data. Rather than being problematic, this fact indicates that the model is applicable to a wider range of cases than represented in the field areas. It also appears that the reasons for adjustment of valley bottom width and the maintenance of a finite depth of sediment on the valley floor are similar in the model and the field, where measured in-channel bedrock incision rates far exceed landscape denudation rates [*Stock et al.*, 2005]. The results indicate that, in active

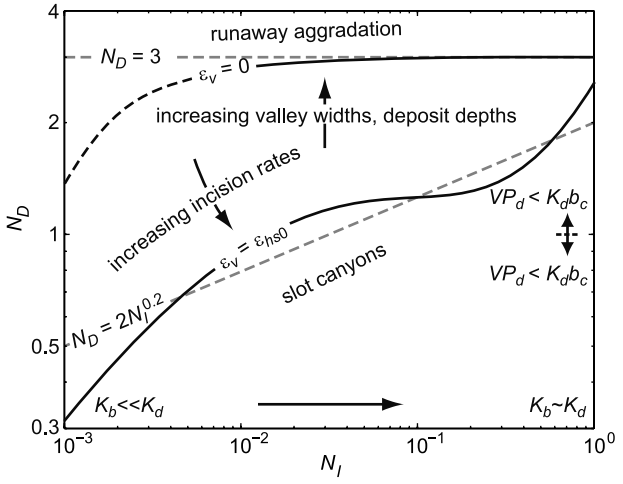

Figure 9. Schematic diagram of model sensitivities with respect to the N_I–N_D parameter space. Black solid and dashed lines represent the best bounds on the steady state region of parameter space. Gray dashed lines represent the approximate bounds given in the text.

orogens with actively incising channels, deposition can drive the formation of accommodation space.

5.1. Conceptual Model of Valley Incision

[45] The field data and simulation results support the following conceptual model of the interaction among episodic deposition, gradual evacuation, and valley form adjustment over geologic time. Just as increased sediment supply forces gradients to steepen over geologic time and thereby transport that supply downstream [e.g., *Whipple and Tucker*, 2002], episodic sediment supply that typically exceeds the short-term fluvial transport capacity forces valley bottoms to widen and thereby increase accommodation space for storage of sediment until it is evacuated.

[46] Bank erosion in small mountain streams typically accomplishes little lateral migration; rather, the streams mainly cut straight down. Without lateral movement the "optimal" valley form might be deep storage, a deep, narrow valley. But the channels do move laterally, not by slow, continuous migration but by discrete "hops" or avulsions, which are caused by debris flow deposition and wood jam formation [e.g., *Lancaster and Grant*, 2006]. Moreover, streams in active orogens such as the OCR must erode bedrock often enough that valley bottom lowering at least keeps pace with hillslope lowering.

[47] A channel will incise to the base of a deposit, and erode bedrock, between avulsions if and only if the deposit is locally thin enough for the channel to do so in the time allowed between those avulsions. Where a deposit is too thick for the channel to incise to bedrock before avulsion, the bedrock will not be eroded. Also, debris flow deposits typically inundate narrow valley bottoms so that the deposits are wider on top than at the bottom. This wider top gives the channel a wider initial platform with each depositional event until some steady state between deposition and evacuation is reached (or not, runaway aggradation is also possible). Moreover, if these wide-topped deposits filled in initially narrow, V-shaped valleys with sloped sides, then the deposits would be thinner at the edges than in the middle, and the channel would be more likely to incise to the base of the deposit and attack the bedrock at those edges. If the relative probability of the channel incising near the sides of the valley is great enough, the shape of the bedrock cross section beneath the sediment will tend to flatten because the shallower sides will be eroded more often than the deeper center.

[48] Valleys with episodic debris flow deposition and avulsing channels will therefore tend to become wide and flat: wide enough to accommodate the imposed sediment in deposits that are thin enough for channels to incise between avulsions, and flat enough for the probability of incision to the base to be roughly equivalent across the entire cross section. Some role of lithologic structure in the evolution of flat valley bottoms cannot be completely ruled out, and the bedrock in the field sites is typically shallowly dipping [*Peck*, 1961]. Some of the toe slopes observed in the field reveal the jagged edges of plucked blocks. However, structure cannot explain other places where transitions are smoother, and the model produces its cross sections without any effect of structure (Figure 6).

[49] For bedrock channels that essentially span the entire valley floor, the mechanism of partial shielding when supply exceeds transport capacity might also explain some of the variation in channel width with varying incision rates and stream gradients [e.g., *Montgomery*, 2004; *Finnegan et al.*, 2005]. The high frequency of channel shifting relative to the time required to incise a depth into bedrock corresponding, say, to the mean deposit volume and the relative ease of incising deposits are important to the carving out of a single valley bottom. Otherwise, the channel might carve so-called epigenetic channels, which are essentially secondary valleys formed when channels are pushed up onto hillslopes by deposition and incise into bedrock there.

[50] The model does lack some key elements of realism, and these missing elements may account for differences in outcomes such as average sediment depths that are perhaps slightly too large. In the model, incision of the deposit proceeds immediately upon deposition, whereas in the field that incision must often wait for decay or break up of deposit-impounding debris dams [e.g., *Lancaster and Grant*, 2006]. In the model, the channel changes position only in response to deposition events and always "chooses" the lowest point on the valley bottom. In the field, debris dams formed by fallen or floating logs can force the channel to change course and incise a new location in the absence of significant new deposition. Some of the model parameter values are arbitrary and bear uncertain relationships to corresponding quantities in the field, but the simple model outcomes of valley bottoms with widths and sediment depths adjusting to deposition and toe slope heights adjusting to incision rate suggest that, despite any deficiencies, the model does elucidate processes active in the field.

5.2. Sensitivities of Processes and Morphologies

[51] For greater bedrock incision rates relative to the deposit incision rate (i.e., greater N_I) and deposition rates that are low relative to rates of sediment evacuation (i.e., smaller N_D), incision by channels outpaces hillslope lowering and produces slot canyons with depths increasing throughout simulations, and such valley cross sections do

not reach steady state (Figure 9). For relatively large deposition rates ($N_D \rightarrow 3$), hillslope lowering outpaces channel incision so that whole cross sections flatten, cease lowering at an appreciable rate, and again do not reach steady state. In the approximate region $2\ N_I^{0.2} \leq N_D \leq 3$ (Figures 5 and 9), hillslope lowering and channel incision achieve parity, finite sediment depths are maintained, and steady state valley cross sections are attained.

[52] Individual simulations lack degrees of freedom present in the field, but the ensemble of simulations presented here shows the kinds of adjustments that are possible. In particular, aggradation in real valleys may steepen alluvial gradients such that evacuation rates may keep pace with further deposition. Given enough time, bedrock profiles will steepen in response to continued higher rates of sediment supply (or become more gradual in response to incision outpacing deposition). Through such steepening, both the bedrock and deposit incision rates, K_b and K_d, will increase and thereby keep the incision number, N_I, approximately the same (equation (3)) and lower the deposition number, N_D (equation (4)), and keep it in a range for which continued bedrock incision is possible.

[53] At steady state, valley bottom lowering by channel incision equals hillslope lowering by soil production, or $\varepsilon_v = \varepsilon_{hs}$, where ε_{hs} is the soil production rate. This condition effectively sets average deposit depths above any oversteepened toe slopes (Figure 8) and, given deposit depths, the heights that these toe slopes reach before hillslope lowering can keep up. Deposition number, N_D, determines valley widths, and N_D and nominal bedrock incision rate, K_b, determine valley bottom lowering rates, and the latter determine rates of hillslope soil production (i.e, bedrock lowering) at which cross sections reach steady state. Hillslope bedrock lowering rates are, in turn, determined by the soil, or deposit, thickness.

[54] Valley bottom lowering may truncate the bedrock at the toe of the hillslope (Figure 6), but does not always oversteepen the surface topography because deposits may fill this valley bottom accommodation space. With greater incision rates and smaller deposit thicknesses, however, heights of oversteepened toe slope bedrock are greater than deposit depths on average, so that fluctuations in those depths less often lead to covering of the bottom parts of hillslopes with sediment. With less frequent covering, hillslope bedrock lowering rates can increase, dependent on soil depth, near the bases of the hillslopes. Furthermore, lowering rate at the base of a slope determines the lowering rate for the rest of the slope.

[55] For small enough N_D and large enough K_b, valley bottom lowering rates exceed the maximum hillslope bedrock lowering rate, the hillslopes cannot keep up with valley incision, oversteepened toe slope heights increase without bound to form slot canyons, and for real valleys, the bedrock on the hillslopes must be lowered by a mechanism (e.g., bedrock landsliding or slab failure) other than the gradual physical weathering included in the present model. In the model, slot canyon depths are dependent on the ratio, $\varepsilon_v/\varepsilon_{hs0}$. For $\varepsilon_v/\varepsilon_{hs0} > 1$, simulations end when valley bottoms have incised twice the initial relief (for steady state simulations, ridge tops must also lower by two such ''relief cycles''). Therefore, slot canyon depths are determined by how far hillslopes can lower during the times for canyons to incise those two relief cycles. As N_D becomes small, valley bottom widths decrease but can get no smaller than the channel width, b_c, and with widths fixed, average deposit depths are therefore even more sensitive to N_D. As slot canyons deepen, valley capacities, $Z_{ts}w$, become arbitrarily large, and $Z_{ts}w/V$ is inversely dependent on deposition number, N_D (equation (4)). These low-N_D sensitivities of normalized valley capacity and deposit depth may therefore be artificial: whereas channel widths in the model are fixed, real channels with greater incision rates will typically be narrower [*Lavé and Avouac*, 2001; *Duvall et al.*, 2004; *Amos and Burbank*, 2007; *Whittaker et al.*, 2007a, 2007b].

[56] Conversely, for large N_D and smaller K_b, valley bottom lowering rates are small, valley sides lack oversteepened toe slopes and are more gradual, soil transport rates are smaller, and soils are thick enough that hillslope bedrock lowering rates are small enough to match the small valley bottom lowering rates. In extreme cases, cross sections approach the horizontal or effectively cease evolution as deposits overtop the ridges. In the natural system, either the episodic deposition driving this whole process would cease as slopes decreased, or the stream profile would eventually steepen enough for the valley to resume lowering.

[57] While valley bedrock gradients can steepen in response to increased sediment supply in areas with active relative rock uplift, the speed of that adjustment is limited by rock uplift rate (for steady state landscapes, equal to the basin-wide denudation rate, [e.g., *Whipple and Tucker*, 1999]). Because streams on bedrock can typically incise at short-term rates far surpassing basin-wide denudation rates (i.e., $\varepsilon_v/K_b \ll 1$; Figures 7 and 8; [*Stock et al.*, 2005]), valley widths adjust more rapidly to increased sediment supply than do valley bedrock gradients. Valley width is therefore likely to be the primary degree of freedom of the bedrock morphology, especially in response to temporal fluctuations in sediment supply with periods that are short relative to the time for gradient steepening through rock uplift. Where an increase in sediment supply overwhelms a valley's capacity to widen while still incising, rock uplift will eventually steepen the gradient so that fluvial processes can more quickly evacuate sediment and incise bedrock. In real valleys, greater bedrock incision rates could also be achieved by narrowing of the channel, similar to the adjustments found in response to tectonic forcing [*Lavé and Avouac*, 2001; *Duvall et al.*, 2004; *Amos and Burbank*, 2007; *Whittaker et al.*, 2007a, 2007b].

[58] At the field sites, much of the variation in normalized valley width and sediment depth is explained by local variations in sediment supply: the larger widths and depths tend to be at confluences of tributaries that contribute debris flows. The sediment storage and unit stream power proxy data (Figure 3) indicate that some bedrock profile steepening may have occurred at locations of greater supply. These data are noisy, and the correspondences between peaks in storage and peaks in unit stream power proxy are inconsistent, but significant discrepancy is not surprising given the episodicity of sediment inputs in Bear Creek and, hence, the likely temporal variation of sediment storage—the measured sediment storage values represent a snapshot in time.

5.3. Steady State and Adjustment to Forcing

[59] Whether the Oregon Coast Range or some parts thereof are at steady state is perhaps immaterial to the question: is steady state possible in a system with so many stochastic elements, with episodic random inputs of sediment that overwhelm the fluvial system such that sediments may spend hundreds to thousands of years in fans and terraces in the valley bottom before channel processes (fluvial or debris flow) finally evacuate them [*Lancaster and Casebeer*, 2007], and where debris dams impound sediment to force alluviation of reaches for decades to centuries [*Montgomery et al.*, 1996, 2003; *Hogan et al.*, 1998; *Lancaster and Grant*, 2006; *Montgomery and Abbe*, 2006]? The model presented here indicates that a steady state in which valley bottom lowering matches ridge top lowering is possible if the valley bottom lowering rate is averaged over enough time.

[60] According to the model, "enough time" may be longer than the duration of the Holocene. Low-frequency fluctuations in valley bottom lowering rate for the simulations in Figure 6 have periods of ~200–400 ka, whereas the period between deposition events is ~2–10 a on average. For a lowering rate of 10^{-4} m/a and the parameters from Table 2, the exponential decay scale for the hillslopes to adjust to changes in base level lowering rate is 70 ka [*Roering et al.*, 2001]. Whether or not these long-period fluctuations are related to the time for hillslope equilibrium, the model results suggest that lowering rates of "steady state" valleys undergo dramatic fluctuations over a range of timescales up to times greater than the hillslope adjustment time.

[61] Techniques for measuring lowering rates effectively average those rates over the times for exhumation of a rock thickness dependent on the method. For cosmogenic radionuclides (e.g., ^{10}Be), that thickness is ~0.8 m (for a material density of $\sim 2 \times 10^3$ kg/m^3 [e.g., *Reneau and Dietrich*, 1991; *Heimsath et al.*, 2001]), and for a lowering rate of 10^{-4} m/a (see below), that thickness corresponds to an averaging time of 8 ka [*Lal*, 1991]. The period of the low-frequency fluctuations in simulated valley bottom lowering is therefore greater than the averaging time for cosmogenic radionuclides in the OCR.

[62] This long period is also comparable to the period of glacial maxima in the Quaternary. It may be, then, that episodic sediment delivery of the kind modeled here could effectively mask the effects of changes in average climate over times of ~100 ka, and it is all the more remarkable that denudation rates estimated from several years of sediment yields ($5–8 \times 10^{-5}$ m/a [*Reneau and Dietrich*, 1991]), hollow infilling and bedrock exfoliation rates ($7–9 \times 10^{-5}$ m/a [*Reneau and Dietrich*, 1991]), and cosmogenic radionuclides ($1.2–1.4 \times 10^{-4}$ m/a [*Bierman et al.*, 2001; *Heimsath et al.*, 2001]) are all comparable. It is also possible that fluctuations akin to those in the simulations presented here may account for some of the discrepancies in the above estimates.

[63] The model results suggest that episodic deposition rates that overwhelm fluvial processes in the short-term force the development of wide valleys over the longer term. The results also suggest that the widths of those valleys are far more sensitive to the relative rate of infilling than to the instantaneous fluvial incision rate or even the long-term valley bottom lowering rate: for long-term average incision rates spanning only a factor of 2, valley widths span a factor of 10 (and sediment depths a factor of 4; Table 4). Valley bottom widths may therefore be poor indicators of relative incision rates where sediment supply is episodic and that episodicity is spatially variable. That is, valleys with the same long-term lowering rate and sediment flux may have different valley widths and average sediment depths depending on the local rate of episodic deposition, e.g., by debris flows. Note that the model does not account for any effects of fluvial sediment supply: incision of deposits is effectively detachment limited. Such an assumption is likely warranted in many mountain streams, where in the absence of obstructions, stream profiles are more than steep enough to transport all fluvial supply [cf. *Montgomery et al.*, 2003; *Lancaster and Grant*, 2006].

[64] My finding that valley widths are sensitive to relative deposition rate is generally consistent with the finding by *Finnegan et al.* [2007] that width of incision increased with greater sediment flux in an experimental channel with substrate designed to mimic bedrock and the finding of *Turowski et al.* [2008] that widening of the Liwu River, Taiwan, may be attributed to alluvial covering of the bed.

6. Conclusions

[65] In three surveyed valley reaches with similar lithology in the Oregon Coast Range, normalized valley widths (w/b_c), which vary over 1.36–16.9, and average deposit depths (H_v), which vary over 0–4.36 m, lack consistent, systematic variation with contributing area. Ranges of deposit depths are nearly identical for the three sites, and average depths, 1–2 m, and normalized widths, 5–7, are similar among the sites. While not conclusive, these results are consistent with the hypothesis that local influences on episodic sediment supply (e.g., tributary junctions) dominate variation in normalized valley bottom widths and average sediment depths within and among these similar sites.

[66] The model of valley cross-section evolution presented here produces a range of morphologies, including flat, deposit-covered valley bottoms and abrupt transitions to valley sides with oversteepened toe slopes, as observed at the field sites and similar sites in the OCR. The model of valley cross-section evolution demonstrates that episodic deposition that temporarily overwhelms fluvial capacity leads to the evolution of accommodation space for sediment through adjustment of valley bottom widths (e.g., Figure 6). Valley bottom width adjustments allow sediment from episodic deposition to be spread across valleys and, hence, average sediment depths to be thin enough for incision through the sediment and into the bedrock below by the channel during times between depositional events. Valley bottom widths and average sediment depths are primarily sensitive to and increase with deposition number (equation (4)).

[67] Through the adjustment of both valley bottom widths and oversteepened toe slope heights, simulated valleys attain steady states in which ridge top and valley bottom bedrock lowering rates are, on average, equal. At steady state, the ratio of long-term average valley bottom lowering and instantaneous incision rates are also primarily sensitive

to and decrease with the dimensionless deposition number. Normalized valley capacity, $Z_{ts}w/V$, increases with incision number (equation (3)) and decreases with deposition number with comparable sensitivities, but steady state solutions are found for a much wider range of incision numbers, which therefore appears to dominate this ratio's sensitivity. The model produces steady state valley cross sections for incision numbers varying over 3 orders of magnitude and for deposition numbers varying over less than 1 order of magnitude.

[68] Headwater valley width, then, apparently adjusts to sediment supply that is episodic, inundates valley bottoms, and is spatially heterogeneous, and that adjustment allows deposit depth to remain relatively shallow such that the channel regularly incises deposits to erode bedrock. The evolution of wide valleys relative to channel width is consistent with *Stock et al.*'s [2005] finding that rates of incision of bedrock channels far exceed basin-wide lowering rates: those bedrock incision rates must be high in order to accomplish long-term lowering of the entire valley floor, which is frequently shielded by deposits with residence times on the order of 10^2–10^3 a [*Lancaster and Grant*, 2006; *Lancaster and Casebeer*, 2007], and the fact that those incision rates are high means that width adjustment is faster than gradient adjustment. Also, growth of oversteepened toe slopes causes lowering rates of valley sideslopes to adjust to valley bottom lowering rates, because these sideslopes must lower via physical weathering that is dependent on the depth of sediment cover, and greater toe slope heights lead to less frequent covering of valley sideslopes by episodic deposition. While this study does not explicitly address the problem of channel width variation [e.g., *Stark and Stark*, 2001], the results do show how width and, more broadly, valley bottom accommodation space for sediment emerge as fundamental degrees of freedom in landscape evolution.

Notation

a exponential decay scale of soil production with soil depth [L^{-1}].
A contributing area [L^2].
A_n amplitude of white noise added to deposit surfaces [L].
b_c channel width, equal to horizontal discretization [L].
F_E function fit to ε_v/K_b *versus* N_I and N_D [dimensionless].
F_H function fit to H_v *versus* N_I and N_D [L].
F_V function fit to $Z_{ts}w/V$ *versus* N_I and N_D [dimensionless].
F_w function fit to w *versus* N_I and N_D [L].
F_{wH} function fit to ε_v/K_b *versus* w and H_v [dimensionless].
H_{hs} average depth of hillslope soil [L].
H_v average depth of valley bottom deposits [L].
K_b bedrock incision rate [L/T].
K_d deposit incision rate [L/T].
K_{hs} nonlinear diffusion constant for hillslope transport [L^2/T].
l horizontal length of simulation domain, or ridge-to-ridge distance [L].
N_D deposition number (see equation (4)) [dimensionless].
N_I incision number (see equation (3)) [dimensionless].
N_{TS} transverse slope number (see equation (5)) [dimensionless].
P_d mean depositional event frequency [T^{-1}].
R^2 fraction of variance explained by a fitted function [dimensionless].
S stream gradient or slope [dimensionless].
S_c critical slope parameter in the nonlinear diffusion model [dimensionless].
V mean volume of depositional events per downstream distance [L^2].
w valley bottom width [L].
Z ridge top-to-valley bottom bedrock relief [L].
Z_{ts} average height of toe slopes [L].
Δx horizontal discretization [L].
ε_{hs} ridge top bedrock lowering rate [L/T].
ε_{hs0} maximum soil production rate [L/T].
ε_v valley bottom bedrock lowering rate [L/T].
ρ_r bulk density of weathered bedrock [M/L^3].
ρ_s bulk density of soil and sediment [M/L^3].
σ_S standard deviation of transverse slope of deposit surfaces [dimensionless].

[69] **Acknowledgments.** The USDA Forest Service Pacific Northwest Research Station and National Science Foundation grants EAR-0545768 and EAR-0643353 provided funding for this study. Nathan Casebeer assisted with model development. Shannon Hayes, John Green, Simon Mudd, Christine May, and Robin Beebee assisted with field work. Thorough reviews by Greg Tucker, Elizabeth Safran, Mikaël Attal, and an anonymous reviewer helped greatly improve the paper.

References

Ahnert, F. (1987), Process-response models of denudation at different spatial scales, *Catena*, *10*, 31–50.
Allen, P. A., and N. Hovius (1998), Sediment supply from landslide-dominated catchments: Implications for basin-margin fans, *Basin Res.*, *10*(1), 19–35, doi:10.1046/j.1365-2117.1998.00060.x.
Almond, P., J. Roering, and T. C. Hales (2007), Using soil residence time to delineate spatial and temporal patterns of transient landscape response, *J. Geophys. Res.*, *112*, F03S17, doi:10.1029/2006JF000568.
Amos, C. B., and D. W. Burbank (2007), Channel width response to differential uplift, *J. Geophys. Res.*, *112*, F02010, doi:10.1029/2006JF000672.
Bierman, P., E. Clapp, K. Nichols, and M. W. Caffee (2001), Using cosmogenic nuclide measurements in sediments to understand background rates of erosion and sediment transport, in *Landscape Erosion and Evolution Modeling*, edited by R. S. Harmon and W. W. Doe III, pp. 89–115, Kluwer Acad., New York.
Bridgman, P. W. (1922), *Dimensional Analysis*, 112 pp., Yale Univ. Press, New Haven, Conn.
Buckingham, E. (1915), Model experiments and the form of empirical equations, *Trans. ASME*, *37*, 263–296.
Drake, A. W. (1967), *Fundamentals of Applied Probability Theory*, 283 pp., McGraw-Hill, New York.
Duvall, A., E. Kirby, and D. Burbank (2004), Tectonic and lithologic controls on bedrock channel profiles and processes in coastal California, *J. Geophys. Res.*, *109*, F03002, doi:10.1029/2003JF000086.
Finnegan, N. J., G. Roe, D. R. Montgomery, and B. Hallet (2005), Controls on the channel width of rivers: Implications for modeling fluvial incision of bedrock, *Geology*, *33*(3), 229–232, doi:10.1130/G21171.1.
Finnegan, N. J., L. S. Sklar, and T. K. Fuller (2007), Interplay of sediment supply, river incision, and channel morphology revealed by the transient evolution of an experimental bedrock channel, *J. Geophys. Res.*, *112*, F03S11, doi:10.1029/2006JF000569.
Flint, J. J. (1974), Stream gradient as a function of order, magnitude, and discharge, *Water Resour. Res.*, *10*, 969–973, doi:10.1029/WR010i005p00969.
Formento-Trigilio, M. L., D. W. Burbank, A. Nicol, J. Shulmeister, and U. Rieser (2003), River response to an active fold-and-thrust belt in a convergent margin setting, North Island, New Zealand, *Geomorphology*, *49*, 125–152, doi:10.1016/S0169-555X(02)00167-8.

Garman, S. L., S. A. Acker, J. L. Ohmann, and T. A. Spies (1995), Asymptotic height-diameter equations for twenty-four tree species in western Oregon, *Res. Contrib. 10*, 22 pp., For. Res. Lab., Corvallis, Oreg.

Hancock, G. S., and R. S. Anderson (2002), Numerical modeling of fluvial strath-terrace formation in response to oscillating climate, *Geol. Soc. Am. Bull.*, *114*, 1131–1142.

Heimsath, A. M., W. E. Dietrich, K. Nishiizumi, and R. C. Finkel (2001), Stochastic processes of soil production and transport: Erosion rates, topographic variation, and cosmogenic nuclides in the Oregon Coast Range, *Earth Surf. Processes Landforms*, *26*, 531–552, doi:10.1002/esp.209.

Hogan, D. L., S. A. Bird, and M. A. Hassan (1998), Spatial and temporal evolution of small coastal gravel-bed streams: Influence of forest management on channel morphology and fish habitats, in *Gravel-Bed Rivers in the Environment*, edited by P. C. Klingeman et al., pp. 365–392, Water Resour. Publ., Highlands Ranch, Colo.

Hovius, N., C. P. Stark, H. T. Chu, and J. C. Lin (2000), Supply and removal of sediment in a landslide-dominated mountain belt: Central Range, Taiwan, *J. Geol.*, *108*, 73–89, doi:10.1086/314387.

Howard, A. D. (1994), A detachment-limited model of drainage basin evolution, *Water Resour. Res.*, *30*(7), 2261–2285, doi:10.1029/94WR00757.

Iverson, R. M. (1997), The physics of debris flows, *Rev. Geophys.*, *35*(3), 245–296, doi:10.1029/97RG00426.

Lal, D. (1991), Cosmic ray labeling of erosion surfaces: In situ nuclide production rates and erosion models, *Earth Planet. Sci. Lett.*, *104*, 424–439, doi:10.1016/0012-821X(91)90220-C.

Lancaster, S. T., and N. E. Casebeer (2007), Sediment storage and evacuation in headwater valleys at the transition between debris-flow and fluvial processes, *Geology*, *35*, 1027–1030, doi:10.1130/G239365A.1.

Lancaster, S. T., and G. E. Grant (2006), Debris dams and the relief of headwater streams, *Geomorphology*, *82*, 84–97, doi:10.1016/j.geomorph.2005.08.020.

Lancaster, S. T., S. K. Hayes, and G. E. Grant (2001), Modeling sediment and wood storage and dynamics in small mountainous watersheds, in *Geomorphic Processes and Riverine Habitat*, *Water Sci. Appl. Ser.*, vol. 4, edited by J. M. Dorava et al., pp. 85–102, AGU, Washington, D. C.

Lancaster, S. T., S. K. Hayes, and G. E. Grant (2003), Effects of wood on debris flow runout in small mountain watersheds, *Water Resour. Res.*, *39*(6), 1168, doi:10.1029/2001WR001227.

Lavé, J., and J. P. Avouac (2001), Fluvial incision and tectonic uplift across the Himalayas of central Nepal, *J. Geophys. Res.*, *106*(B11), 26,561–26,591, doi:10.1029/2001JB000359.

May, C. L., and R. E. Gresswell (2003), Processes and rates of sediment and wood accumulation in headwater streams of the Oregon Coast Range, USA, *Earth Surf. Processes Landforms*, *28*, 409–424, doi:10.1002/esp.450.

May, C. L., and R. E. Gresswell (2004), Spatial and temporal patterns of debris-flow deposition in the Oregon Coast Range, USA, *Geomorphology*, *57*(3–4), 135–149, doi:10.1016/S0169-555X(03)00086-2.

Miller, D. J., and L. E. Benda (2000), The two-meter rule: Fluvial terrace construction under punctuated sediment supply, *Geol. Soc. Am. Abstr. Programs*, *32*(7), 118.

Montgomery, D. R. (2004), Observations on the role of lithology in strath terrace formation and bedrock channel width, *Am. J. Sci.*, *304*, 454–476, doi:10.2475/ajs.304.5.454.

Montgomery, D. R., and T. B. Abbe (2006), Influence of logjam-formed hard points on the formation of valley-bottom landforms in an old-growth forest valley, Queets River, Washington, USA, *Quat. Res.*, *65*, 147–155, doi:10.1016/j.yqres.2005.10.003.

Montgomery, D. R., T. B. Abbe, J. M. Buffington, N. P. Peterson, K. M. Schmidt, and J. D. Stock (1996), Distribution of bedrock and alluvial channels in forested mountain drainage basins, *Nat.*, *381*, 587–589, doi:10.1038/381587a0.

Montgomery, D. R., K. M. Schmidt, H. M. Greenberg, and W. E. Dietrich (2000), Forest clearing and regional landsliding, *Geology*, *28*(4), 311–314, doi:10.1130/0091-7613(2000)28<311:FCARL>2.0.CO;2.

Montgomery, D. R., T. M. Massong, and S. C. S. Hawley (2003), Influence of debris flows and log jams on the location of pools and alluvial channel reaches, Oregon Coast Range, *Geol. Soc. Am. Bull.*, *115*(1), 78–88, doi:10.1130/0016-7606(2003)115<0078:IODFAL>2.0.CO;2.

Muto, T., and R. J. Steel (1997), Principles of regression and transgression: The nature of the interplay between accommodation and sediment supply, *J. Sediment. Res.*, *67*(6), 994–1000.

Peck, D. L. (1961), Geologic map of Oregon west of the 121st meridian, *U.S. Geol. Surv. Misc. Invest.*, *Map I-325*.

Personius, S. F. (1995), Late Quaternary stream incision and uplift in the forearc of the Cascadia subduction zone, western Oregon, *J. Geophys. Res.*, *100*(B10), 20,193–20,210, doi:10.1029/95JB01684.

Personius, S. F., H. M. Kelsey, and P. C. Grabau (1993), Evidence for regional stream aggradation in the central Oregon Coast Range during the Pleistocene-Holocene transition, *Quat. Res.*, *40*, 297–308, doi:10.1006/qres.1993.1083.

Reneau, S. L., and W. E. Dietrich (1991), Erosion rates in the southern Oregon Coast Range: Evidence for an equilibrium between hillslope erosion and sediment yield, *Earth Surf. Processes Landforms*, *16*, 307–322, doi:10.1002/esp.3290160405.

Rice, S., and M. Church (1996), Bed material texture in low order streams on the Queen Charlotte Islands, British Columbia, *Earth Surf. Processes Landforms*, *21*, 1–18, doi:10.1002/(SICI)1096-9837(199601)21:1<1::AID-ESP506>3.0.CO;2-F.

Roering, J. J., J. W. Kirchner, and W. E. Dietrich (1999), Evidence for nonlinear, diffusive sediment transport on hillslopes and implications for landscape morphology, *Water Resour. Res.*, *35*(3), 853–870, doi:10.1029/1998WR900090.

Roering, J. J., J. W. Kirchner, and W. E. Dietrich (2001), Hillslope evolution by nonlinear, slope-dependent transport: Steady state morphology and equilibrium adjustment timescales, *J. Geophys. Res.*, *106*(B8), 16,499–16,513, doi:10.1029/2001JB000323.

Roering, J. J., J. W. Kirchner, and W. E. Dietrich (2005), Characterizing structural and lithologic controls on deep-seated landsliding: Implications for topographic relief and landscape evolution in the Oregon Coast Range, USA, *Geol. Soc. Am. Bull.*, *117*, 654–668, doi:10.1130/B25567.1.

Schlager, W. (1993), Accommodation and supply—A dual control on stratigraphic sequences, *Sediment. Geol.*, *86*, 111–136, doi:10.1016/0037-0738(93)90136-S.

Snyder, N. P., K. X. Whipple, G. E. Tucker, and D. J. Merritts (2000), Landscape response to tectonic forcing: Digital elevation model analysis of stream profiles in the Mendocino triple junction region, northern California, *Geol. Soc. Am. Bull.*, *112*(8), 1250–1263, doi:10.1130/0016-7606(2000)112<1250:LRTTFD>2.3.CO;2.

Stark, C. P., and G. J. Stark (2001), A channelization model of landscape evolution, *Am. J. Sci.*, *301*, 486–512, doi:10.2475/ajs.301.4-5.486.

Stock, J., and W. E. Dietrich (2003), Valley incision by debris flows: Evidence of a topographic signature, *Water Resour. Res.*, *39*(4), 1089, doi:10.1029/2001WR001057.

Stock, J. D., D. R. Montgomery, B. D. Collins, W. E. Dietrich, and L. Sklar (2005), Field measurements of incision rates following bedrock exposure: Implications for process controls on the long-profiles of valleys cut by rivers and debris flows, *Geol. Soc. Am. Bull.*, *117*(1), 174–194, doi:10.1130/B25560.1.

Swanson, F. J., M. M. Swanson, and C. Woods (1977), Inventory of mass erosion in the Mapleton Ranger District, Siuslaw National Forest, report, For. Sci. Lab., Corvallis, Oreg.

Turowski, J. M., N. Hovius, M.-L. Hsieh, D. Lague, and M.-C. Chen (2008), Distribution of erosion across bedrock channels, *Earth Surf. Processes Landforms*, *33*, 353–363, doi:10.1002/esp.1559.

Underwood, E. F. (2007), Sediment transfer and storage in headwater basins of the Oregon Coast Range: Transit-times from ^{14}C dated deposits, M. S. thesis, 55 pp., Oreg. State Univ., Corvallis, Oreg.

VanLaningham, S., A. Meigs, and C. Goldfinger (2006), The effects of rock uplift and rock resistance on river morphology in a subduction zone forearc, Oregon, USA, *Earth Surf. Processes Landforms*, *31*, 1257–1279, doi:10.1002/esp.1326.

Weissmann, G. S., G. L. Bennett, and A. L. Lansdale (2005), Factors controlling sequence development on Quaternary fluvial fans, San Joaquin Basin, California, USA, in *Alluvial Fans: Geomorphology, Sedimentology, Dynamics*, *Geol Soc. Spec. Publ. Ser.*, vol. 251, edited by A. M. Harvey et al., pp. 169–186, Geol. Soc. of London, London.

Whipple, K. X., and G. E. Tucker (1999), Dynamics of the stream-power river incision model: Implications for height limits of mountain ranges, landscape response timescales, and research needs, *J. Geophys. Res.*, *104*(B8), 17,661–17,674, doi:10.1029/1999JB900120.

Whipple, K. X., and G. E. Tucker (2002), Implications of sediment-flux-dependent river incision models for landscape evolution, *J. Geophys. Res.*, *107*(B2), 2039, doi:10.1029/2000JB000044.

Whittaker, A. C., P. A. Cowie, M. Attal, G. E. Tucker, and G. P. Roberts (2007a), Bedrock channel adjustment to tectonic forcing: Implications for predicting river incision rates, *Geology*, *35*(2), 103–106, doi:10.1130/G23106A.1.

Whittaker, A. C., P. A. Cowie, M. Attal, G. E. Tucker, and G. P. Roberts (2007b), Contrasting transient and steady state rivers crossing active normal faults: New field observations from the Central Apennines, Italy, *Basin Res.*, *19*(4), 451–632, doi:10.111/j.1365-2117.2007.00337.x.

S. T. Lancaster, Department of Geosciences, Oregon State University, 104 Wilkinson Hall, Corvallis, OR 97331-5506, USA. (stephen.lancaster@geo.oregonstate.edu)